Separation Science and Technology
Publication details, including instructions for authors and subscription information:
http://www.informaworld.com/smpp/title~content=t713708471

Treatment of Oily Waste Water Using Low-Cost Ceramic Membrane: Flux Decline Mechanism and Economic Feasibility

B. K. Nandi[a]; R. Uppaluri[a]; M. K. Purkait[a]
[a] Department of Chemical Engineering, Indian Institute of Technology Guwahati, Guwahati, Assam, India

To cite this Article Nandi, B. K. , Uppaluri, R. and Purkait, M. K.(2009) 'Treatment of Oily Waste Water Using Low-Cost Ceramic Membrane: Flux Decline Mechanism and Economic Feasibility', Separation Science and Technology, 44: 12, 2840 — 2869
To link to this Article: DOI: 10.1080/01496390903136004
URL: http://dx.doi.org/10.1080/01496390903136004

Separation Science and Technology, 44: 2840–2869, 2009

ISSN: 0149-6395 print/1520-5754 online
DOI: 10.1080/01496390903136004

Taylor & Francis
Taylor & Francis Group

Treatment of Oily Waste Water Using Low-Cost Ceramic Membrane: Flux Decline Mechanism and Economic Feasibility

B. K. Nandi, R. Uppaluri, and M. K. Purkait
Department of Chemical Engineering, Indian Institute of Technology Guwahati, Guwahati, Assam, India

Abstract: This work addresses the applicability of different membrane pore blocking models for the prediction of flux decline mechanisms during dead end microfiltration (MF) of stable oil-in-water (o/w) emulsions using relatively low-cost ceramic membranes. Circular disk type membranes (52.5 mm diameter and 4.5 mm thickness) were prepared by the paste method using locally available low-cost inorganic precursors such as kaolin, quartz, calcium carbonate, sodium carbonate, boric acid, and sodium metasilicate. Characterization of the prepared membrane was done by SEM analysis, porosity determination, and pure water permeation through the membrane. Hydraulic pore diameter, hydraulic permeability, and hydraulic resistance of the membrane was evaluated as 0.7 μm, $1.94 \times 10^{-6}\,m^3/m^2 \cdot s \cdot kPa$ and $5.78 \times 10^{11}\,m^2/m^3$, respectively. The prepared membrane was used for the treatment of synthetic stable o/w emulsions of 40 and 50 mg/L crude oil concentration in batch mode with varying trans-membrane pressure differentials ranging from 41.37 to 165.47 kPa. The membrane exhibited 96.97% oil rejection efficiency and $21.07 \times 10^{-6}\,m^3/m^2 \cdot s$ permeate flux after 30 min of experimental run at 165.47 kPa trans-membrane pressure for 50 mg/L oil concentration. Different pore blocking, models such as complete pore blocking, standard pore blocking, intermediate pore blocking and cake filtration were used to gain insights into the nature of membrane fouling during permeation. The observed trends for flux decline data convey that the decrease in permeate flux was initially due to intermediate pore blocking (during 1 to 10 minutes of

Received 8 December 2008; accepted 12 May 2009.
Address correspondence to R. Uppaluri or M. K. Purkait, Department of Chemical Engineering, Indian Institute of Technology Guwahati, Guwahati 781039, India. Tel.: +91-361-2582262; Fax: 91-361-2582291. E-mail: ramgopalu@iitg.ernet.in or mihir@iitg.ernet.in

experimental run) followed with cake filtration (during 10 to 30 minutes of experimental run). Based on retail prices of the inorganic precursors, the membrane cost was estimated to be 130 $/m^2. Finally, preliminary process economic studies for a single stage membrane plant were performed for the application of the prepared membrane in industrial scale treatment of o/w emulsions. A process economics study inferred that the annualized cost of the membrane plant would be 0.098 $/m^3 feed for treating 100 m^3/day feed with oil concentration of 50 mg/L.

Keywords: Ceramic membrane, microfiltration, oily wastewater, pore blocking, process economics

INTRODUCTION

Various process industries such as petroleum refineries, petrochemical industries, metallurgical, transportation, and food processing industries produce large volumes of oily wastewater with oil concentrations of 50 to 1000 mg/L. Existing tolerance limits of total oil and grease concentrations in wastewater streams is 10 mg/L (1). To achieve the desired discharge limits, among various alternative plausible technologies, membrane technology has been found to be very promising due to various advantages such as lower capital cost, higher separation factors, compact design, and the elimination of other chemical and mechanical treatment units. Recent research indicates that both polymeric membranes as well as ceramic membranes can be applied for the treatment of o/w emulsions (2). However, during filtration, polymeric membranes are susceptible to fouling and degradation and eventually need to be replaced frequently. As a result the operating cost increases significantly (2). In addition, each polymeric membrane has its own solvent compatibility and weakness to specific chemicals present in the permeating liquid. For instance, cellulose acetate membranes are severely affected by the presence of chlorine and solvents such as acetone and aniline (3). On the other hand, due to high chemical, thermal, and mechanical stability, ceramic membranes appear to more promising for the treatment of o/w emulsions for industrial scale operation. One of the limitations for industrial application of the ceramic membrane is their cost, which is significantly higher (2000 to 4000 $/m^2 (4)) than polymeric membranes (50 to 200 $/m^2 (3)). The higher cost of ceramic membranes is due to the utilization of expensive inorganic precursors such as alumina and zirconia and higher sintering temperature (more than 1100°C) during membrane fabrication (5,6). This is also due to the fact that higher sintering temperatures demand higher electrical energy and hence operating costs. In addition, higher sintering temperatures may also give rise to

enhancement in furnace power specifications and hence the installed costs. Therefore, higher sintering temperatures translate to higher membrane fabrication costs.

To circumvent the higher costs of inorganic membranes, existing and ongoing research in the preparation of low-cost inorganic membranes is quite challenging as the use of low-cost inorganic precursors as well as the low sintering temperature (below 1000°C) may deteriorate the membrane performance, lifetime, and ultimately affect their edge over the polymeric membranes. Fortunately, many literatures do indicate that kaolin-based membranes have the ability to serve as low-cost substitutes when compared to costly alumina and zirconia membranes. Belouatek et al. (7), and Almandoza et al. (8), have prepared kaolin-based ceramic membrane applicable for microfiltration (MF) or ultrafiltration (UF) applications. However, the sintering temperature used in these works was more than 1100°C. As a result, the cost of the inorganic membrane is anticipated to be higher due to higher sintering temperatures, even though inexpensive raw materials were utilized. Therefore, there exists a necessity to address the fabrication of stable inexpensive ceramic membranes that involves both cheaper precursors and lower sintering temperatures (lower than 1000°C), to further existing research trends in cheaper ceramic membrane filters.

Most of the literatures that report the treatment of oily wastewaters address technological solutions for feed oil concentrations ranging 500 to 2000 mg/L (2). These feed systems consist of unstable oil droplets of droplet sizes higher than 50 μm and hence their removal is easily achievable (9). However, lower droplet sizes (less than 10 μm) exist for feeds with oil concentrations below 100 mg/L. These sub-micron range oil droplets have been reported to be highly stable and their separation is anticipated to be a challenging one (10). Therefore, it is very likely that the oil concentrations in discharged process wastewater streams from effluent treatment plants fail to comply with the allowable discharge limits of 10 mg/L (1). For such complicating scenarios, ceramic membrane technology could provide technological solutions. To the best of our knowledge, the applicability of low cost ceramic membranes to treat wastewaters consisting of oil concentration below 100 mg/L and their economic feasibility has not been studied to date. This work attempts to address these issues using a low-cost MF ceramic membrane.

The objective of this work was to identify competent, low-cost inorganic precursor formulation that can yield ceramic membrane using a sintering temperature below 1000°C to yield an inexpensive ceramic membrane. Different low-cost inorganic raw materials such as kaolin,

quartz, calcium carbonate, sodium carbonate, boric acid, and sodium metasilicate were used for the preparation of the ceramic membrane. The sintering temperature was kept below 900°C to minimize the cost of the fabrication process without affecting the performance of the membranes. The cost of the fabricated ceramic membranes was estimated to be 130 $\$/m^2$ based on the retail price of inorganic precursors. Subsequently, the membrane cost was assumed to be 400 $\$/m^2$ including fabrication and module costs, which is significantly comparable to that of the conventional polymeric membranes (50–200 $\$/m^2$) and far lower than other commercially available ceramic membranes (2000–4000 $\$/m^2$). Structural, morphological, and pure water flux (PWF) study of the prepared membrane was carried out to evaluate the general characteristics of the fabricated ceramic membrane. PWF experiments were carried out to evaluate different membrane parameters such as hydraulic permeability, hydraulic pore diameter, and porosity of the membrane. Prepared inexpensive inorganic membrane was used to verify the separation of o/w emulsions capability with low concentrations (40 and 50 mg/L). Permeate flux decline was analyzed using various flux decline models to get an insight into the nature of membrane fouling during filtration. Finally, preliminary studies on the cost of the prepared membranes along with the process economics of the membrane for a single stage membrane plant was adopted to evaluate the economic competitiveness of the prepared membrane in industrial scale treatment systems. Thereby, we wish to promote further the applicability of ceramic membrane technology in challenging industrial scenarios.

EXPERIMENTAL

Raw Materials

This work utilized six common inorganic raw materials such as kaolin (CDH, India), quartz (Research Lab Fine Chem Industry, India), calcium carbonate (Merck India), sodium carbonate (Merck India), boric acid (Merck India), and sodium metasilicate (SD Fine Chem Ltd., India). All these raw materials used for inorganic fabrication were graded at least 99.5% pure and were used without any further purification. Different raw materials used in this work for the fabrication of inorganic membrane served for different functional attributes. Kaolin provided low plasticity and high refractory properties to the membrane. Quartz contributed to the mechanical and thermal stability of the membrane. Regulation of porous texture in the ceramic was realized by calcium carbonate which

under sintering conditions would dissociate into CaO and release CO_2 gas. The path taken by the released CO_2 gas thereby created the porous texture of the inorganic membrane and contributed to the membrane porosity during the sintering process. Boric acid increased membrane mechanical strength by the formation of metallic metaborates at sintering temperatures. Boric acid and sodium carbonate also act as colloidal agents and improved the dispersion properties of the inorganic precursors thereby addressing homogeneity in the membrane structure. In a similar way, sodium meta-silicate acted as a binder by creating silicate bonds among the elements to induce higher mechanical strength in the ceramic membrane (11).

Two major clay materials namely kaolin and quartz used for the membrane fabrication process were characterized using X-ray diffraction analysis (Make: Bruker Axs; Model: D8 ADVANCE) and particle size distribution analysis (Make: Malvern; Model: Mastersizer 2000). The XRD spectrum of the clay materials matched with the JCPDS database file PDF-01-089-6538 and PDF-01-075-0443 for kaolin and quartz. The results obtained from particle size analysis of clay materials infers that particle size of the kaolin varied from 18.67 to 0.224 μm and 37.24 μm to 1.18 μm for quartz. The average particle size of kaolin and quartz were 2.37 and 8.4 μm, respectively.

Membrane Fabrication

The ceramic micrifiltration (MF) membrane was prepared from a clay mixture with the composition as kaolin (8 g), quartz (3 g), calcium carbonate (5 g), sodium carbonate (2 g), boric acid (1 g) and sodium metasilicate (1 g). Subsequently, the raw materials were mixed with 7 g of distilled water to prepare a paste. Details of the preparation method are shown in Fig. 1. The paste was molded in the form of a circular disk on a gypsum surface by using an SS 316 ring of 55 mm internal diameter and 5 mm thickness. Then the disk type mold was dried at room temperature for 24 hours, at 100°C for 12 hours and at 250°C for 24 hours for complete removal of loose moisture. Subsequently, the membrane was sintered at 850°C for 5 hours with a heating rate of 2°C per minute. A sintering temperature of 850°C was chosen based on thermogravimetric analysis of the clay mixture, where no major phase transformation was observed above 843°C (12). After sintering, the membranes achieved a hard, rigid, and porous texture. Eventually, the membrane was polished with silicon carbide abrasive paper (C-220) to obtain a smooth, flat MF membrane of diameter 52.5 mm and thickness 4.5 mm. Finally, the membrane was cleaned in a sonicator for 15 minutes to remove loose

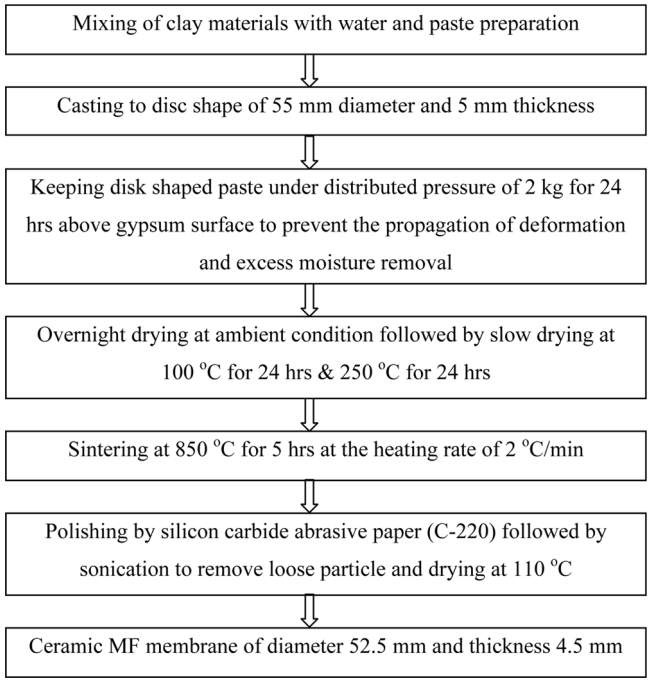

Figure 1. Block diagram for the preparation of ceramic membrane from raw materials.

particles from the membrane, dried at 120°C, and was ready for the MF experiment.

Characterization Techniques

The prepared membrane was characterized by scanning electron microscopy (SEM) analysis, total porosity determination, and hydraulic permeability determination using pure water permeation through the membrane. Scanning electron microscopy (Make: Oxford; Model: LEO 1430VP) was carried out to analyze the presence of possible defects and estimate the membrane pore size. The estimation of the average membrane pore size (d_s) from SEM micrographs was carried out using ImageJ software (Version 1.40) (13). The open porosity of the membrane was evaluated using the Archimedes method with water as the wetting liquid. Pure water flux (PWF) permeation experiments were carried out for the determination of the hydraulic permeability (P_m), hydraulic pore diameter (d_l) of the membrane.

Experimental Set-Up

A schematic of the experimental set-up used for both air and water permeation experiments is presented in Fig. 2. The set-up constitutes a Teflon tubular cell (125 ml capacity) with a flat circular Teflon base plate that houses the composite membrane. Membranes were kept in the Teflon casing and sealed with epoxy resin. For air permeation experiments the outlet was connected to a gas flow meter for measuring the gas flow rate for various trans-membrane pressure drop of air. For pure water flux and o/w emulsions the feed (deionized water and o/w emulsions) was filled in the tubular section from the top. The cell was pressurized with compressed air. The liquid permeate flow rate was measured using a digital weight machine. The membrane diameter was 52.5 mm and effective membrane area was $1.66 \times 10^{-3}\,m^2$. Before using each fresh membrane, compaction of the membrane was performed using deionized water at a transmembrane pressure of 310 kPa (which is higher than the maximum operating pressure for the set of experiments conducted). During these experiments, the membrane flux was observed to be high initially and reduced to a near steady value after two hours of operation for all the membranes.

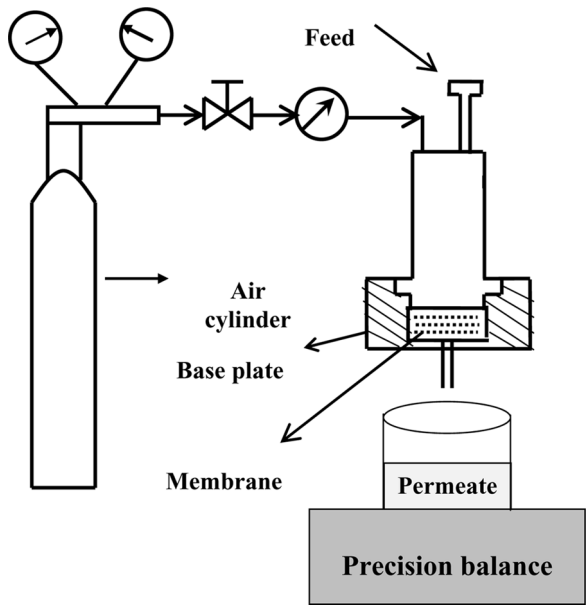

Figure 2. Schematic of the experimental set-up.

Preparation of Oil-in-Water Emulsions

Crude oil collected from Guwahati Refinery, Indian Oil Corporation Limited (IOCL), India, was used without any treatment to prepare synthetic o/w emulsions. The crude oil was obtained from Assam crude oil reservoirs. Assam crude is typically characterized to possess a high degree of aromatic and wax content (14). Oil-in-water emulsions were prepared using distilled water and crude oil by placing the o/w mixture in a sonicator tank (Make: Elmasonic; Model: S30H) for 15 hours at a temperature of 25°C. The disappearance of the oily layer on the water surface confirmed the achievement of emulsification process during sonication. No surfactant was added externally to stabilize the emulsion as the natural surfactants present in the crude oil were sufficient to yield a highly stable emulsion. The onset of the stable emulsion was further tested by measuring the droplet size distribution, the absorbance at 235 nm wavelength, the pH, and the viscosity of the emulsions regularly. After a time period of two weeks, coalescence of the oil droplets were observed that lead to the formation of a thin oil film on the water surface. Similar observations were also found by Huotari et al. (15). Therefore, all MF experiments were done with emulsions prepared within 10 days. Droplet sizes and their distribution of the prepared o/w emulsions were measured using a laser particle size analyzer (Make: Malvern; Model: Mastersizer 2000). The droplet sizes of the emulsion were observed to vary between 0.04 μm to 10 μm. The average droplet sizes of the emulsions were 0.52 and 0.56 μm for emulsions prepared with 40 and 50 mg/L oil concentration, respectively.

Microfiltration of Oil-in-Water Emulsion

Microfiltration experiments of the synthetic oil-in-water (o/w) emulsions were carried out in an unstirred batch MF cell using two different concentrations of oil (40 and 50 mg/L). Four different trans-membrane pressures differential (ΔP) of 41.37, 82.74, 124.11, and 165.47 kPa are used to observe the effect of ΔP on the permeate flux and oil rejection efficiency. The feed concentration of oil was measured before each MF run. The permeate was collected at an interval of 5 minutes for the determination of permeate oil concentration. The permeate flux was calculated at an interval of 1 minute using an electronic balance place at the bottom of the MF cell. Further, all MF experiments were conducted at room temperature

(~25°C). The permeate flux (J, $m^3/m^2 \cdot s$) and the percent oil rejection (R) were evaluated using the following expressions:

$$J = \frac{V}{A \times \Delta t} \tag{1}$$

$$R = \left(1 - \frac{C_P}{C}\right) \times 100 \tag{2}$$

Where A (m^2) is the effective membrane area, V (m^3) is the volume of permeate, Δt (s) is the sampling time, C (mg/L) and C_P (mg/L) are the concentration of oil in the feed and permeate, respectively. The oil concentrations in the permeate and the feed were determined using a UV-Vis spectrophotometer (Make: Perkin Elmer Precisel; Model: Lambda 35) by measuring absorbance at a wave length of 235 nm where maximum absorbance was observed (10). After each experimental run, the membranes were cleaned with "Surfexcel," a laboratory detergent solution. The pure water flux (PWF) of each membrane was verified before and after cleaning the membrane. The difference between the PWF of cleaned membrane and fresh membrane was found to be negligible. All these quantitative experiments were conducted for at least four different membrane samples in order to confirm the average membrane performance characteristics. The maximum uncertainty in all measurements was within the range of ±5%.

Analysis of Fouling Mechanism

Hermia (16) developed four empirical models for dead-end filtration based on constant pressure filtration laws that correspond to four basic types of flux decline mechanisms: complete blocking, intermediate blocking, standard blocking and cake filtration (Fig. 3). During constant pressure dead end MF, initial permeate flux mainly depends on the membrane resistance. As microfiltration proceeds, different phenemona take place across the membrane structure such as, adsorption of oil droplets on ceramic matrix causing blocking of pores, oil cake deposition and concentration polarization. All these phenomena contribute to the overall resistance of the membrane and as a result MF permeation process could involve a transition from a membrane resistance-limited regime to a pore blocking resistance-limited or a cake resistance-limited regime. Thereby, the evaluations of parameters associated to these four basic models of flux decline enable physical insights and comprehensions upon the most appropriate mechanisms applicable for the process.

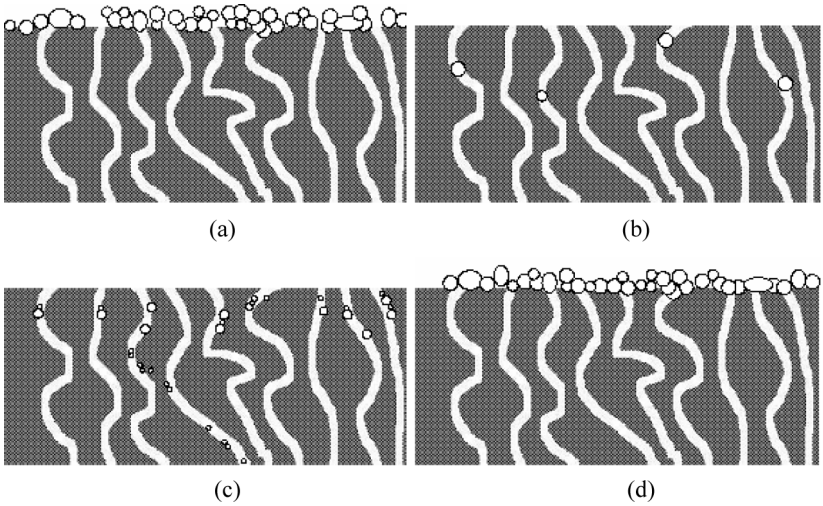

Figure 3. Schematic representation of blocking mechanism (a) Intermediate pore blocking, (b) Complete pore blocking, (c) Standard pore blocking and (d) Cake filtration.

Intermediate Pore Blocking Model

This model considers that one membrane pore is not necessarily blocked by one oil droplet and some oil droplets may settle over others. The non-blocked membrane surface diminishes with time and hence the probability of blocking a membrane pore reduces by oil droplet continuously with time. Intermediate blocking occurs when the oil droplet size is similar to the membrane pore size. Therefore, oil droplets are expected to obstruct a membrane pore entrance without blocking the pore completely (Fig. 3a). The permeate flux decline model based on the intermediate blocking mechanism is expressed as (3,17)

$$J = J_0(1 + K_I\ AJ_0t)^{-1} \tag{3}$$

Complete Pore Blocking Model

According to this model, it is assumed that each oil droplet arriving at the membrane surface participates in blocking by pore sealing and the oil droplets never settle over another that has been previously deposited on the membrane surface. The permeate flux through the

unblocked pores is unaffected and hence the fractional reduction in the permeate flux is equal to the fractional reduction in the membrane surface area corresponding to unblocked pores. This type of fouling occurs when the size of the oil droplets is greater than the size of the membrane pores. Therefore, pore blocking takes place over the membrane surface and not inside the membrane pores (Fig. 3b). Applicable flux decline expression for complete pore blocking model is presented as (3,17)

$$J = J_0 \exp(-k_b t) \tag{4}$$

Standard Pore Blocking Model

This model considers that oil droplets enter the membrane pores and deposit over the pore walls due to the irregularity of the pore passages, thereby reducing the membrane pore volume. Some oil droplets are not simply deposited over the internal surface of the membrane pores since they are adsorbed over the pore walls. This type of fouling is caused by oil droplets smaller than the membrane pore size and pore blocking occurs inside the membrane pores. As a result, the volumes of membrane pores decreases proportionally to the filtered permeate volume (Fig. 3c). The decrease in the volume of membrane pores with time is equal to the decrease in their cross section. The permeate flux expression for standard pore blocking model is expressed as (3,17)

$$J = J_0 \left(1 + 0.5 K_S (A J_0)^{0.5} t\right)^{-2} \tag{5}$$

Cake Filtration Model

Cake filtration usually occurs when particles larger than the average pore size accumulate on the membrane surface, forming a "cake" (Fig. 3d). With time the cake grows and provides an additional porous barrier through which the liquid must permeate. As a result, the cake may increase the particle removal efficiency of the membrane; however, it also increases the membrane resistance and subsequently diminishes flux. The permeate flux for this case is expressed as (3,17)

$$J = J_0 \left(1 + 2 K_S (A J_0)^2 t\right)^{-2} \tag{6}$$

Identification of Fouling Mechanism

A linearized representation of Eqs. (3) – (6) is shown below:

a) Intermediate pore blocking model: $J^{-1} = J_0^{-1} + k_i t$ (7)

b) Complete pore blocking model: $\ln(J^{-1}) = \ln(J_0^{-1}) + k_b t$ (8)

c) Standard pore blocking model: $J^{-0.5} = J_0^{-0.5} + k_s t$ (9)

d) Cake filtration model: $J^{-2} = J_0^{-2} + k_c t$ (10)

where $k_i = K_I A$, k_b, $k_s = 0.5 K_S A^{0.5}$ and $k_c = 2K_C A^2$ are the system parameters relating to intermediate pore blocking, complete pore blocking, standard pore blocking, and cake filtration model, respectively. Therefore, a plot of J^{-1} vs. t, $\ln(J^{-1})$ vs. t, $J^{-0.5}$ vs. t and J^{-2} vs. t shall be a straight line with slope of k_i, k_b, k_s, k_c and y-intercept of $J_0^{-1}, \ln(J_0^{-1})$, $J_0^{-0.5}$ and J_0^{-2} for intermediate pore blocking, complete pore blocking, standard pore blocking, and cake filtration model, respectively. The appropriate applicability of these models can be confirmed by comparing the values of coefficient of correlation (R^2) obtained from the linear regression analysis as well as error analysis between experimental and calculated flux data.

Process Economics

In general, the total cost of a membrane-based process is evaluated as the sum of different cost components such as cost of the membranes, pumps, pipes and valves, electrical and instrumentation, tanks and frames, and other miscellaneous items (including buildings, electrical supply, treated water storage, and pumping, etc.). However, as the aim of the present study was a conceptual cost-based economic study, different establishment costs (buildings, electrical supply, treated water storage, and pumping etc.) were ignored and only the cost of the membrane, the pump (used to energize stream from feed tank to higher pressure membrane chamber), and the operating cost of the pump (electricity) were considered in this study. The main focus of this study was to find the effect of membrane cost, operating pressure, and feed concentration on the total operating cost of the plant. Annualized cost of the membrane (Q_{Amem}, \$/year), pump (Q_{Apump}, \$/year) and operating cost of the pump (Q_{AOpump}, \$/year) were estimated using the

Table 1. Different model equations for the cost estimation (20)

Item	Expressions	Eq. no
Membrane area	$A_{mem} = \frac{Q_F \times \theta}{J_{ss}},\ J_{SS} = f(\Delta P)$	(11,12)
Annualized cost of membrane module	$Q_{Amem} = \frac{(A_{mem})^{0.8} \times Q_{mem} \times i \times (i+1)^{L_M}}{(i+1)^{L_M} - 1}$	(13)
Pump cost	$Q_{pump} = I \times f_1 \times f_2 \times L \times 81.27 \times (C \times \Delta P)^{0.39}$	(14)
Annualized cost of the pump	$Q_{Apump} = \frac{Q_{pump} \times i \times (i+1)^{L_p}}{(i+1)^{L_p} - 1}$	(15)
Work done by the pump	$W = \Delta Z \times g + \frac{v^2}{2} + \frac{\Delta P}{\rho}, v = \frac{Q_F}{\frac{\pi}{4} d_{pipe}^2}$	(16, 17)
Energy required by the pump	$E = \left(\frac{W \times Q_F \times \rho_E}{\beta}\right)$	(18)
Annualized operating cost of the pump	$Q_{AOpump} = E \times 24 \times 300 \times Q_E$	(19)
Total annualized cost of the plant	$Q_{total} = Q_{Amem} + Q_{Apump} + Q_{AOpump}$	(20)
	$Q_{total} = f(C, \Delta P, \theta, Q_F, Q_{mem})$	(21)

correlation provided by Sethi and Wiesner (18) and are summarized in Table 1.

The annualized cost of the membrane (Q_{Amem}, \$/year) was evaluated as a function of the membrane area (A_{mem}, m^2) required to obtain the desired permeate flux, the module cost of the membrane (Q_{mem}, \$/m^2), and the life span (L_M, years) of the membrane. The annualized pump cost (Q_{AOpump}, \$/m^2) was calculated as functions of the update factor (I), the labor factor (L), the construction material factor (f_1), the suction pressure correction factor (f_2), the feed concentration (C), and the trans-membrane pressure differential (ΔP). The operating cost of the membrane plant was evaluated as a function of the power (energy, E, kW) required by the pump to provide necessary flow rate and trans-membrane pressure differential. Finally, the total annualized cost of the plant (Q_{total}) was evaluated as the sum of the cost of the membrane unit (Q_{Amem}), the cost of pump (Q_{Apump}), and the operating cost of the pump (Q_{AOpump}) and was a function of C, ΔP, θ, Q_F, Q_{mem} where other parameters were assumed to be constant. In the present study, Q_{total} were optimized as a single variable function of ΔP for feed oil concentration of 50 mg/L and varying steady feed flow rate of 1 to 100 m^3/day. Details of the other parameters used in this work are summarized in Table 2. Relevant update factors have been considered to report costs based on the prices of year 2008.

Table 2. Different design and operating parameters used for process optimization and economic analysis (20)

Parameter	Values
Feed flow rate (Q_F, m^3/day)	1 to 100
Stage cut ratio (θ)	0.8
Height between pump and membrane (ΔZ, m)	3
Density of feed (ρ_F, Kg/m^3)	1000
Acceleration due to gravity (g, m/s^2)	9.81
Efficiency of pump (β)	0.6
Update factor (I)	2.28
Factor to adjust for pump construction material (f_1)	1.5
Factor to adjust for suction pressure range (f_2)	1
Factor used to incorporate labor costs (L)	1.4
Annual interest rate (i)	0.1
Membrane cost (Q_M, \$/m^2)	400
Membrane life (L_M, years)	5
Pump life (L_P, years)	10
Energy cost (Q_E, \$/kWh)	0.1
Diameter of pipe (d_{pipe}, m)	0.05

RESULTS AND DISCUSSION

Characterization of the Membrane

SEM Analysis

Figure 4a shows the SEM image of the prepared membrane. The membrane shows a surface with highly porous, rough morphological structure. A superficial observation of the image indicates that the membrane did not have any defects such as pinholes and cracks. The maximum observable pore size of the surface is about 2.5 μm. Individual pore diameters of the membrane using ImageJ software (Version 1.40) was measured from these types of five images taken from randomly selected locations of the membrane and the average pore diameter and pore size distribution were evaluated. The area average pore diameter (d_s) from SEM analysis of the membrane was evaluated by assuming cylindrical porous texture of the membrane as

$$d_s = \left[\frac{\sum_{i=1}^{n} n_i d_i^2}{\sum_{i=1}^{n} n_i} \right]^{0.5} \tag{22}$$

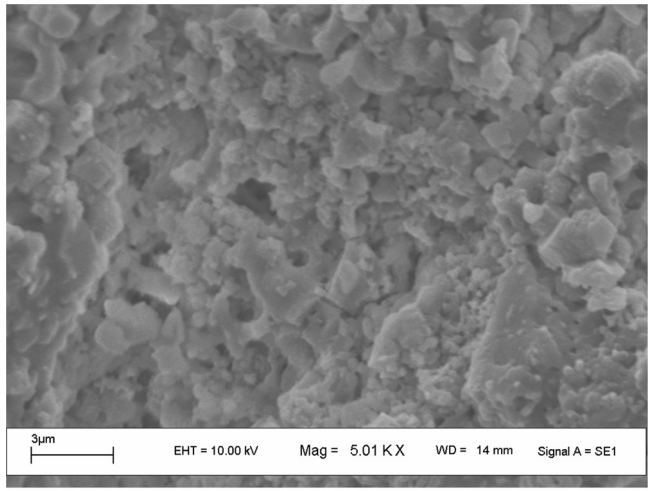

(a)

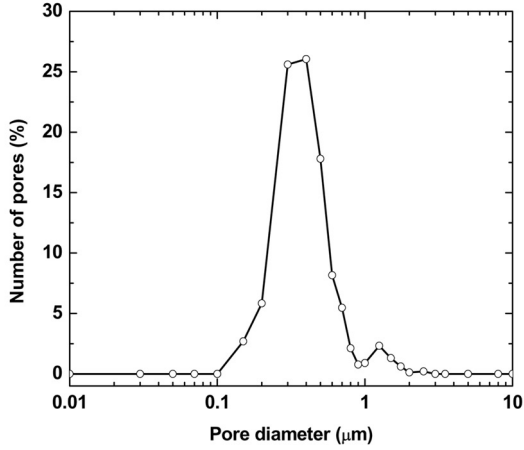

(b)

Figure 4. (a) SEM image of the prepared membrane; (b) Pore size distribution of the prepared membrane obtained from the image analysis.

Where, n is the number of pore, d_i is the pore diameter (μm) of ith pore.

Figure 4b presents the pore size distribution summarizing the evaluated values of percentage pore numbers with respect to different pore diameters. The figure illustrates that about 50% of the pores had a pore diameter in the range of 0.3 to 0.5 μm. The maximum and

minimum pore sizes of the membrane were 2.5 μm (0.2%) and 0.15 μm (2.7 %). Average pore diameter of the membrane (calculated using Eq. (22)) was 0.55 μm.

Hydraulic Permeability, Pore Diameter, and Resistance of the Membrane

The hydraulic permeability (P_m), pore diameter (d_l) and resistance of the membrane (R_m) were evaluated by assuming the presence of cylindrical pores in the membrane matrix using the following expressions (19)

$$PWF = \frac{Q}{S \cdot \Delta t} = P_m \cdot \Delta P \tag{23}$$

$$d_l = 2 \times \left[\frac{8 \times \mu \times l \times P_m}{\varepsilon}\right]^{0.5} \tag{24}$$

$$R_m = \frac{\Delta P}{PWF} \tag{25}$$

Where PWF ($m^3\,m^{-2}\,s^{-1}$) is the liquid flux through the membrane, ΔP (kPa) is the trans-membrane pressure drop across the membrane, μ is the viscosity of water, l is pore length, and $\varepsilon = (n \times \pi \times r_l^2)$ is the total porosity of the membrane. The porosity (ε) of the membrane determined by the pycnometric method using water as wetting liquid was 0.42. The hydraulic permeability of the membrane and corresponding membrane resistance determined from pure water permeation experiment was $1.94 \times 10^{-9}\,m^3/m^2.s.Pa$ and $5.78 \times 10^{11}\,m^2/m^3$. The hydraulic pore diameter calculated from PWF data using Eq. (24) was 0.7 μm which is slightly higher than the pore diameter calculated from SEM analysis. However, this type of deviation is always observed in membrane pore size determination using different techniques and the results are in good agreement with those reported in literature for kaolin-based membrane (8) as well as for polymeric membranes (13).

Microfiltration of Oil-in-Water Emulsion

Effect of Trans-Membrane Pressure and Feed Concentration on Permeate Flux

Figure 5 shows the permeate flux profiles for 50 mg/L crude oil feed concentration with respect to the permeation time for different

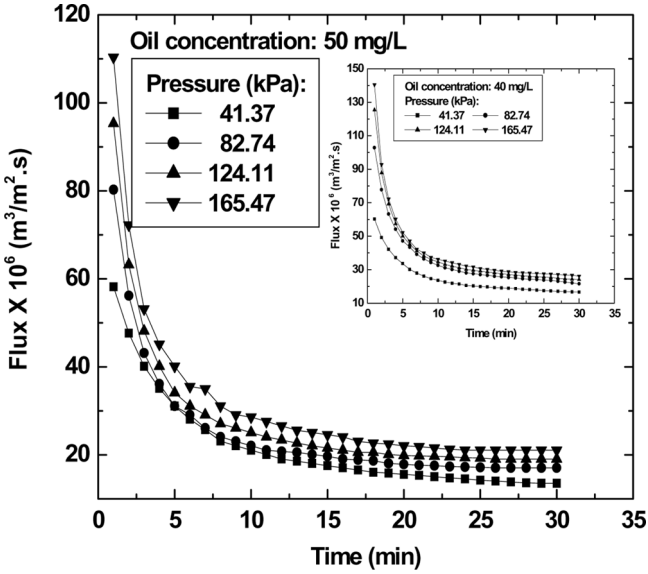

Figure 5. Variation of permeate flux for with time at different trans-membrane pressure. Initial oil concentration: 50 mg/L.

trans-membrane pressure drop (41.37, 82.74, 124.11, and 165.47 kPa). From the figure, it was observed that the permeate flux declined sharply within the initial 10 to 15 minutes of operation and becomes gradual thereafter. The permeate flux decreases from 58.2×10^{-6} to $13.6 \times 10^{-6}\,m^3/m^2 \cdot s$ within 30 minutes of experimental run at a trans-membrane pressure drop of 41.37 kPa. This decline in flux with time was due to pore blocking of the ceramic porous structure and formation of the thin oily film layer over the membrane surface. It is also observed that the permeate flux increases with increase in trans-membrane pressure. From the figure it may be observed that as the permeate flux increased from 58.2×10^{-6} to $110.4 \times 10^{-6}\,m^3/m^2 \cdot s$ when ΔP was increased from 41.37 to 165.47 kPa. An increase in permeate flux with ΔP was due to the higher driving force across the membrane. Similar flux decline trends with trans-membrane pressure and operating time were also observed for 40 mg/L oil concentrations (inset of Fig. 5). The permeate flux was observed to increased with decrease in oil concentration. This was because of the fact that with an increase in feed concentration, adsorptive resistances as well as thin film hydraulic resistances increased and hence the permeate flux decreased.

Effect of Trans-Membrane Pressure and Feed Concentration on Oil Rejection

Figure 6 shows the percent rejection of crude oil with time at four different trans-membrane pressure drops for a feed oil concentration of 50 mg/L. It can be observed from the figure that the rejection efficiency of the membrane slightly increased from 96.9 (5 minute) to 97.3% (30 minute) in the due course of MF test at ΔP of 41.37 kPa. Also, the rejection efficiency was observed to be slightly lower at 165.47 kPa (95.7 to 97%). Similar trends were also observed for oil concentrations of 40 mg/L where the rejection efficiency was varied from 94.9% (41.37 kPa, 5 min) to 95.8% (165.47 kPa, 30 min) studied in this work (inset of Fig. 6). A decrease in the oil rejection efficiency with a reduction in oil concentration was due to the lower droplet size of the oil at lower concentration. A reduction in the oil rejection efficiency with increase in ΔP is argued according to the hypothesis that higher pressures facilitate the enhancement of wetting and coalescence of oil droplets, thereby imposing some oil droplets to pass through the membrane pores and reach the permeate stream. The increase in oil-rejection efficiency with

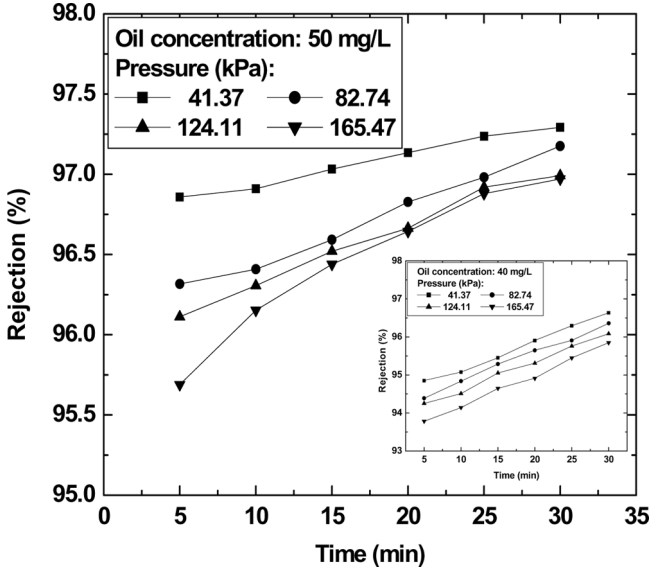

Figure 6. Variation of oil rejection efficiency with time at different trans-membrane pressure. Initial oil concentration: 50 mg/L.

time was due to the reduction of the pore diameter of the membrane as a result of the adsorption of oil droplets in the membrane pores.

Analysis of Membrane Fouling Mechanism

Figures 7 and 8 show the plot of different membrane pore blocking models for both initial oil concentrations (40 and 50 mg/L). The plots correspond to various models such as intermediate filtration (J^{-1} vs. t as outlined by (Eq. 7)), complete pore blocking ($\ln(J^{-1})$ vs. t as outlined in Eq. (8)), standard pore blocking ($J^{-0.5}$ vs. t as outlined by Eq. (9)), and cake filtration models (J^{-2} vs. t as outlined in Eq. (10)). From these figures, it can be observed that the decline in permeate flux can be explained using cake filtration models as the plot of J^{-2} vs. t (Figs. 7d

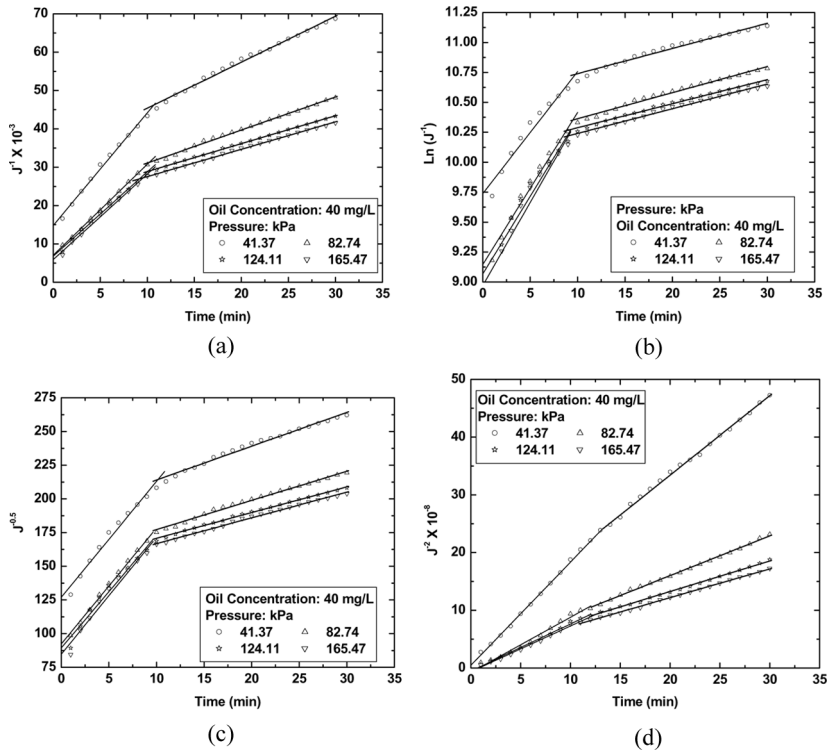

Figure 7. Linear plot of permeate flux vs. time for different pore blocking models (7,19). Initial oil concentration: 40 mg/L. (a) J^{-1} vs. t, (b) $\ln(J^{-1})$ vs. t, (c) $J^{-0.5}$ vs. t, (d) J^{-2} vs. t.

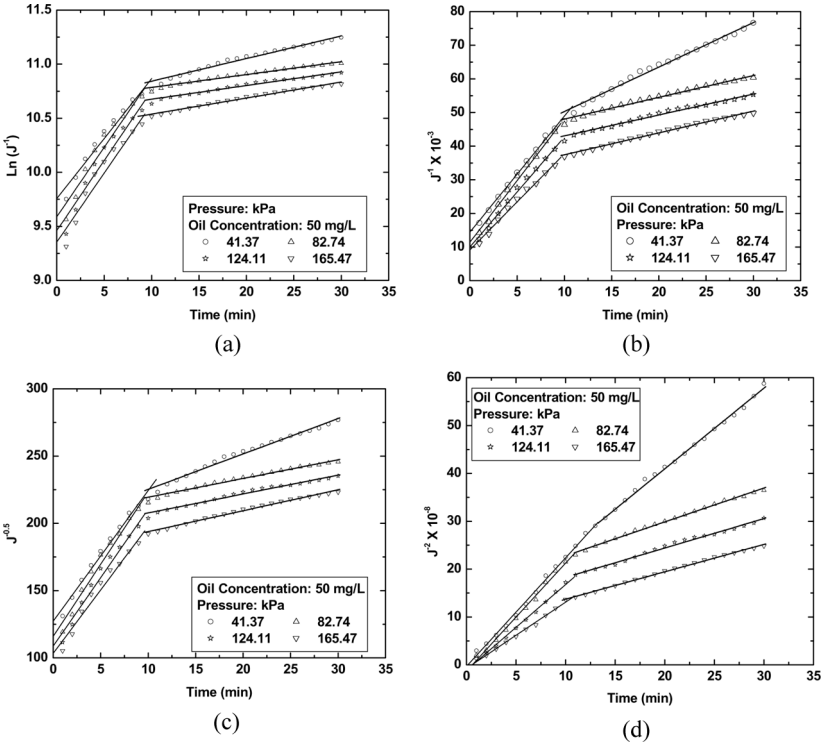

Figure 8. Linear plot of permeate flux vs. time for different pore blocking models (7,19). Initial oil concentration: 50 mg/L. (a) J^{-1} vs. t, (b) $\ln(J^{-1})$ vs. t, (c) $J^{-0.5}$ vs. t, (d) J^{-2} vs. t.

and 8d) gives the best linear fitness. However, a careful observation of the plots indicates that, two different distinct filtration regimes of initial 10 minutes and the rest. It signifies that the flux decline with time occurs through two different pore blocking mechanisms. A similar type of result was also observed during MF of o/w emulsions with a polymeric membrane (17). Henceforth, the experimental flux data was further analyzed separately in the two time regimes, namely the initial regime (during the first 10 minutes of MF) and the later regime (10 to 30 minutes of MF) to identify the most competent combinations of models in both the regimes. Using the linear regression analysis the slope, intercept, as well as correlation coefficients of all the permeate flux data were calculated and summarized in Tables 3a, 3b, and 3c, respectively.

For the initial regime (during the first 10 minutes of MF), it can be critically observed in Table 3b that there exists a negative intercept for

Table 3a. Calculated values of slopes obtained from linear regression analysis of different membrane pore blocking models (Eqs. (7–10))

Concentration of oil (mg/L)	Pressure (kPa)	Complete pore blocking (k_b)		Standard pore blocking (k_S)		Intermediate pore blocking (k_i)		Cake filtration (k_C) $\times 10^{-7}$	
		Initial regime	Final regime	Initial regime	Final regime	Initial regime	Final regime	Initial regime	Final regime
40	41.37	0.102	0.021	8.60	2.51	2940	1199	17.86	13.79
	82.74	0.127	0.022	8.59	2.16	2372	862	9.55	6.88
	124.11	0.129	0.020	8.34	1.91	2200	726	8.15	5.29
	165.47	0.138	0.021	8.67	1.91	2230	713	7.92	4.98
50	41.37	0.111	0.021	9.70	2.63	3447	1323	22.70	16.85
	82.74	0.129	0.012	10.73	0.39	3662	648	22.60	7.07
	124.11	0.130	0.013	10.18	1.40	3268	623	17.88	6.15
	165.47	0.128	0.015	9.44	1.55	2855	650	13.86	5.72

Table 3b. Calculated values of intercept obtained from linear regression analysis of different membrane pore blocking models (Eqs. (7–10))

Concentration of oil (mg/L)	Pressure (kPa)	Complete pore blocking ($\ln(J_0^{-1})$)		Standard pore blocking ($J_0^{-0.5}$)		Intermediate pore blocking (J_0^{-1})		Cake filtration (J_0^{-2}) $\times 10^{-7}$	
		Initial regime	Final regime	Initial regime	Final regime	Initial regime	Final regime	Initial regime	Final regime
40	41.37	9.738	10.529	126.92	188.93	14797	33402	4.84	58.28
	82.74	9.147	10.145	92.36	155.57	7054	22465	−7.5	22.42
	124.11	9.067	10.087	89.41	151.65	6791	21624	−5.12	26.56
	165.47	8.971	10.035	84.76	147.62	5909	20421	−6.38	22.40
50	41.37	9.757	10.632	127.25	198.97	14458	37066	33.35	72.39
	82.74	9.588	10.666	115.95	205.59	11449	41562	13.33	157.27
	124.11	9.461	10.549	108.75	193.75	10038	36814	10.98	121.15
	165.47	9.354	10.390	103.35	178.33	9162	30920	7.6	79.95

Table 3c. Observed values of correlation coefficient (R^2) obtained linear regression analysis of permeate flux data for different membrane pore blocking models (Eqs. (7–10))

Concentration of oil (mg/L)	Pressure (kPa)	Complete pore blocking		Standard pore blocking		Intermediate pore blocking		Cake filtration	
		Initial regime	Final regime	Initial regime	Final regime	Initial regime	Final regime	Initial regime	Final regime
40	41.37	0.956	0.981	0.979	0.988	0.993	0.993	0.997	0.998
	82.74	0.978	0.987	0.995	0.993	0.999	0.996	0.978	0.998
	124.11	0.936	0.994	0.974	0.997	0.994	0.999	0.990	0.998
	165.47	0.930	0.991	0.971	0.995	0.993	0.998	0.991	0.999
50	41.37	0.963	0.980	0.984	0.987	0.995	0.992	0.992	0.997
	82.74	0.943	0.986	0.973	0.989	0.991	0.992	0.992	0.996
	124.11	0.943	0.984	0.974	0.987	0.993	0.989	0.994	0.993
	165.47	0.937	0.986	0.971	0.990	0.991	0.993	0.993	0.998

the cake filtration model. As the negative intercept values signify negative initial permeate flux, so this model cannot be applicable for the flux decline and henceforth is ignored in the subsequent analysis of flux decline for the initial regime. Further, it can be also observed in Table 3c for the same regime that the R^2 values for all other models (standard pore blocking, complete pore blocking, and intermediate pore blocking) is in appreciable range (0.95 to 0.99). To further analyze the applicability of various models, the percent error of experimental flux and predicted permeate flux using slope and intercept values for those models were calculated and analyzed. The percent error of the permeate flux was calculated using the standard equation as:

$$Error(\%) = \left(\frac{J_{Experimental} - J_{Calculated}}{J_{Experimental}}\right) \times 100 \tag{26}$$

Figure 9a shows the result obtained from error analysis for experimental condition of 40 mg/L initial oil concentration and 124.11 kPa trans-membrane pressure drop. Based on the observations from Fig. 9a, it can be inferred that intermediate pore blocking model is the most appropriate model to account for the flux decline mechanism during the initial regime, with the lowest error (−0.0003 to 0.21%). Similar observations were also observed for other experimental conditions also.

Similarly, for the later regime (10 to 30 minutes of MF), it can be observed in Table 3b that none of the models indicate negative intercepts and hence R^2 and error analysis need to be conducted to evaluate the most appropriate model. Based on observed values of R^2 in Table 3c, it can be inferred that all the four models indicated good fitness ($R^2 > 0.99$). Figure 9b shows the result obtained from error analysis for experimental condition of 50 mg/L initial oil concentration and 82.74 kPa trans-membrane pressure drop. Based on the observations from Fig. 9b, it can be inferred that the cake filtration model is the most appropriate to represent the flux decline during the later regime (10 to 30 minutes of MF), with the lowest error (−0.11 to 1.16%). Therefore, based on the physical observation as well as the fitness of the cake filtration model, the thin layer of oil droplets formed during the membrane process can be conveniently represented using a cake layer model.

Figure 10 presents a parity plot between experimental and calculated flux based on the combinations of the two most appropriate models in the initial and later regimes. As shown, a good fitness between experimental and evaluated values is observed and henceforth, the suggested model combination is herewith inferred to be applicable for the analysis,

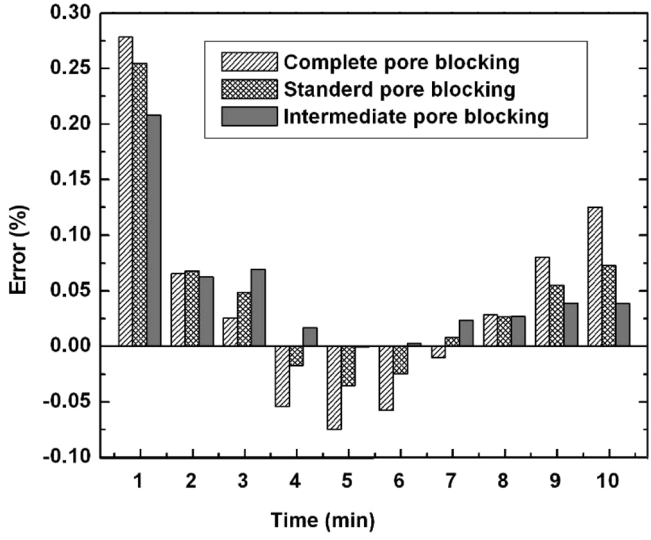

(a)

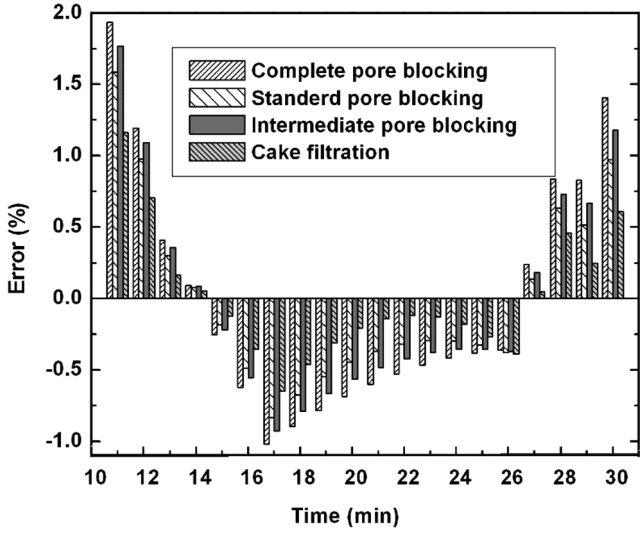

(b)

Figure 9. (a) Variation of error (%) with time for the initial regime. Initial oil concentration: 40 mg/L and trans-membrane pressure: 124.11 kPa; (b) Variation of error (%) with time for the initial regime. Initial oil concentration: 50 mg/L and trans-membrane pressure: 82.74 kPa.

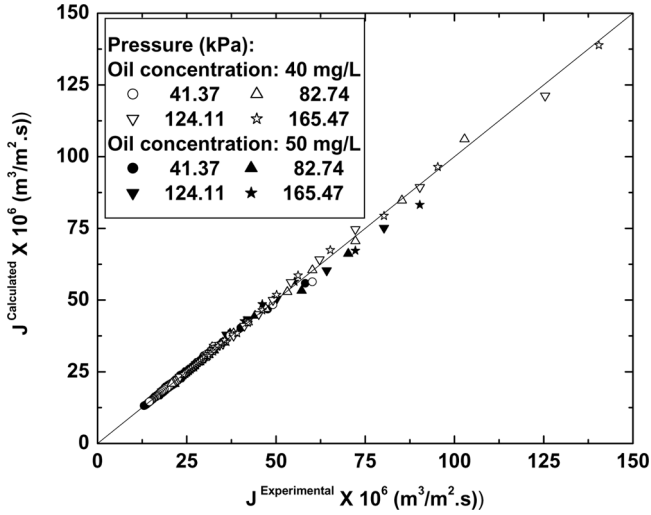

Figure 10. Parity plot of experimental and calculated permeate flux using combination of intermediate pore blocking and cake filtration model.

design, planning, and scheduling of time-dependent MF processes for oil-water emulsion separation in the process industries.

Membrane Cost

The industrially competitive aspect of membrane technology lies in its cost. Based on the unit costs of raw materials used for preparing the inorganic membrane in this work (Table 4), the manufacturing cost of the inorganic membrane was evaluated to be 130 $\$/m^2$. Including manufacturing and shipment costs, the average cost of the inorganic membrane for industrial applications based on bulk production methods would be closer to the value of 400 $\$/m^2$. Contemporary elemental costs of various polymeric membranes and α-alumina ceramic symmetric membrane varies form 50 to 200 $\$/m^2$ (3) and 2000 to 4000 $\$/m^2$ (4), respectively. Therefore, it can be inferred from the cost analysis that the inorganic membrane based on kaolin would be closer to the cost of the polymeric membranes deployed for industrial configurations (as retail cost is much higher than industrial production cost). However, the reported value of the membrane cost is conceptual in nature and may vary significantly depending on the fouling characteristics, on time performance, and

Table 4. Cost analysis of fabricated membrane from the unit cost of raw materials

Material	Weight (gm)	Unit price ($/kg*)	Cost contribution ($/kg mixture)
Kaolin (PDF-01-089-6538)	8	5	2
Quartz (SiO_2) (PDF-01-075-0443)	3	64	9.6
Calcium carbonate ($CaCO_3$)	5	4.2	1.05
Sodium carbonate (Na_2CO_3)	2	4.6	0.46
Boric acid (H_3BO_3)	1	5.6	0.28
Sodium metasilicate ($Na_2SiO_3 \cdot 9H_2O$)	1	8.4	0.42
Water	7	–	
Total 50 numbers of membranes with surface area of 0.108 m^2 (0.02 kg dry mixture/membrane of 4.5 mm thickness and 52.5 mm diameter). So the cost of the membrane is 13.81 $/0.108 $m^2 \approx 130$ $/$m^2$			13.81 ($/kg dry mixture)

*Prices taken from the catalog of the corresponding company as mentioned in experimental section.

long-term stability of the ceramic membrane in particular process applications.

Economic Feasibility

Table 5 presents a variation of the total optimum cost for the treatment of o/w emulsions with feed oil concentration 50 mg/L for varying feed rate. The module cost of cheaper inorganic membrane (including module and installed costs) reported in this work was taken as 400 $/$m^2$ with an

Table 5. Cost contribution of the pump, membrane and operating cost with respect to total cost of the process for different feed rate

Feed (m^3/day)	Operating pressure (kPa)	Total cost ($/$m^3$ feed)	Cost contribution (%)		
			Pump	Membrane	Operating
1	66.43	0.425	44.60	54.37	1.03
10	119.05	0.189	30.89	65.52	3.60
25	139.46	0.143	24.85	69.74	5.41
50	151.37	0.118	20.42	72.55	7.03
100	159.05	0.098	16.32	74.90	8.78

assumption that the overall membrane cost would be higher than the materials cost of 130 $/m^2. As the ceramic membrane offers excellent chemical and fouling resistance, the life span of the membrane was assumed to be 5 years. Permeate flux data after 30 minutes of experimental run were assumed as steady the permeate flux (J_{ss}). Subsequently, J_{ss} was observed to vary linearly with operating pressure and a suitable correlation for both feed oil concentrations were developed and used in Eq. (11) for the evaluation of the required membrane area (A_{mem}). In addition, optimization methodology using a genetic algorithm was applied to yield optimal combinations of the membrane area and the pressure differential (ΔP).

From Table 5, it can be inferred that the total annualized cost for the treatment of 100 m^3/day feed rate will be around 0.098 $/$m^3$ feed with the optimal operating pressure of 159.05 kPa. Further, it can also be observed that with an increase in the feed capacity (from 1 to 100 m^3/day), the cost contribution due to the pump to the overall cost reduced from 44.6 to 16.32% whereas the cost of the membrane increased from 54.37 to 74.9%. The lower contribution of the pump cost to the overall cost is anticipated due to lower optimal trans-membrane pressure differentials for the chosen case. The increase in the operating cost of the plant was observed to be insignificant when compared to the fixed costs of the membrane and pump. A further reduction in the membrane process system cost is anticipated, as the existing steady-state data were based on the dead end MF and not the cross-flow mode of operation. Therefore, based on these observations, it can be inferred that the ceramic membrane based process systems appear to be promising for industrial scale application.

CONCLUSIONS

This work reports an inexpensive ceramic precursor formulation utilizing locally available low-cost inorganic raw materials such as kaolin, quartz, calcium carbonate, sodium carbonate, boric acid, and sodium metasilicate. The average pore size of the prepared ceramic membrane was 0.55 μm with a total porosity of 42%. Based on the retail price of raw materials cost of membranes was estimated to be 130 $/m^2. The membrane shows 97.3% oil rejection efficiency with 13.6×10^{-6} $m^3/m^2 \cdot s$ permeate flux after 30 min of experimental run at 41.37 kPa trans-membrane pressure and 50 mg/L oil concentration. A decline in the permeate flux has been analyzed using different pore blocking models. A decrease in the permeate flux was initially due to (1 to 10 minute) intermediate pore blocking and later (10 to 30 minute) due to

cake filtration. Process economics studies for a single stage membrane permeation unit infers that the total optimal cost of the membrane permeation unit was estimated to be 0.098 $/m^3 feed for processing 100 m^3/day feed of 50 mg/L feed oil concentration and was dominated by the membrane cost. Henceforth, the newly prepared ceramic membrane is suggested for application in oily wastewater treatment using suitable MF/UF techniques.

REFERENCES

1. Bevis, A. (1992) The treatment of oily water by coalescing. *Filtr. Sep.*, 295.
2. Cheryan, M.; Rajagopalan, N. (1998) Membrane processing of oily streams. Wastewater treatment and waste reduction. *J. Membr. Sci.*, *151*: 13.
3. Cheryan, M. (1998) *Ultrafiltration and microfiltration handbook*; Techno. Pub. Co. Inc.
4. Tennison, S. (2000) Current hurdles in the commercial development of inorganic membrane reactors. *Membrane Technology*, *2000* (128): 4.
5. Das, R.; Dutta, B. K. (1999) Permeation and separation characteristics of supported alumina and titania membranes. *Sep. Sci. Technol.*, *34* (4): 609.
6. Saffaj, N.; Persin, M.; Younsi, S.A.; Albizane, A.; Cretin, M.; Larbot, A. (2006) Elaboration and characterization of micro-filtration and ultra-filtration membranes deposited on raw support prepared from natural Moroccan clay: Application to filtration of solution containing dyes and salts. *Appl. Clay Sci.*, *31*: 110.
7. Belouatek, A.; Benderdouche, N.; Addou, A.; Ouagued, A.; Bettahar, N. (2005) Preparation of inorganic supports for liquid waste treatment. *Micropor. and Mesopor. Mater.*, *85*: 163.
8. Almandoza, M.C.; Marchese, J.; Prádanos, P.; Palacio, L.; Hernández, A. (2004) Preparation and characterization of non-supported micro-filtration membranes from aluminosilicates. *J. Membr. Sci.*, *241*: 95.
9. Gryta, M.; Karakulski, K. (1999) The application of membrane distillation for the concentration of oil-water emulsions. *Desalination*, *121*: 23.
10. Chakrabarty, B.; Ghoshal, A.K.; Purkait, M.K. (2008) Ultrafiltration of stable oil-in-water emulsion by polysulfone membrane. *J. Membr. Sci.*, *325*: 427.
11. Reed, J.S. (1995) *Principles of Ceramics Processing*; John Wiley & Sons: NewYork.
12. Wang, M.C.; Wu, N.C.; Hon, M.H. (1994) Preparation of nepheline glass-ceramics dental porcelain. *Materials Chemistry and Physics*, *37*: 370.
13. Chakrabarty, B.; Ghoshal, A.K.; Purkait, M.K. (2008) SEM analysis and gas permeability test to characterize polysulfone membrane prepared with polyethylene glycol as additive. *J. Colloid Interf. Sci.*, *320*: 245.

14. Kandwal, V.C.; Agrawal, K.M.; Nautiyal, S.P.; Khan, H.U. (2000) Paraffin deposition and viscosity temperature behaviour of Assam crude oil. *Petro. Sci. Technol.*, *18*: 755.
15. Huotari, H.M.; Huisman, I.; Tragardh, H.G. (1999) Electrically enhanced crossflow membrane filtration of oily waste water using the membrane as a cathode. *J. Membr. Sci.*, *156*: 49.
16. Hermia, J. (1982) Constant pressure blocking filtration laws–Application to power-law non-newtonian fluids. *Trans. Inst. Chem. Eng.*, *60*: 183.
17. Hu, B.; Scott, K. (2008) Microfiltration of water in oil emulsions and evaluation of fouling mechanism. *Chem. Eng. J.*, *136*: 210.
18. Sethi, S.; Wiesner, M.R. (2000) Simulated cost comparisons of hollow-fiber and integrated nanofiltration configurations. *Wat. Res.*, *34*: 2589.
19. Mulder, M. (1991) *Basic Principles of Membrane Technology*; Kluwer Academic Publishers: Dordrecht.